Brookhaven National Laboratory
Department of Physics
Omega group

Characterization of LGADs and AC-LGADs produced at BNL

Luigi Lavitola

Supervisors:
Alessandro Tricoli
Gabriele Giacomini
Gabriele D'Amen

First version

Upton, NY October 2019

Abstract

This note presents the characterisation of Low-Gain Avalanche Diodes (LGADs) and AC coupled LGADs (AC-LGADs) produced at Brookhaven National Laboratory in the Si-Fab, a class 100 clean room facility. The performance of small test structures with different particle beams are shown, in particular with laser beams and Strontium 90 Beta source.

This notes cover in detail the test of cross-talk for a single pad LGAD, two 3x3 AC-LGAD pixel matrix and a strip AC-LGAD.

Table of Contents

1. Introduction

Future High Energy Physics (HEP) experiments will require particle detectors with a faster time resolution and high radiation-tolerance in order to preserve and increase their tracking and vertexing performances in a challenging environment such as the one a the Large Hadron Collider (LHC). To illustrate the impact of timing information, let us consider a typical situation in HEP collider experiment. Typically, in experiments such as ATLAS (A Toroidal LHC Apparatus) at the LHC, several proton-proton interactions can occur within the time window of one beam crossing (pile- up). Since the space separations among the interaction vertices typically is larger than the resolution of the tracker, tracking informations have been sufficient to reconstruct each event. However this situation will be different after the LHC upgrade when the machine will be pushed in the so-called High-Luminosity phase (HL-LHC). The HL-LHC will begin its operation in 2026 and will provide an instantaneous luminosity of 5 - 7 x 10^{34} $cm^{-2}s^{-1}$ corresponding to approximately 200 inelastic proton-proton interactions per beam crossing, which means almost four times the current pile-up. This number is so large that the vertices in the event will be overlapping in space leading to degradation in the precision of the reconstructed variables and possibly loss of efficiency. The HL-LHC will thus present an extremely challenging environment to the ATLAS experiment, well beyond that for which it was designed. To further illustrate this, an example is presented in Fig.1.1 [1], which shows a single event with 200 interactions in the z-t plane, where each ellipse, which corresponds to an interaction vertex, is 30 ps in time and 1mm in z. The vertical dotted lines indicate the z position of the reconstructed primary vertices while the red ellipse and the red solid line indicate the hard-scatter vertex. It is clear then, from the tracker point of view, vertices occurring at different times but very close in space may lead to ambiguities in the track-to-vertex association. A powerful way to mitigate the effects of pile-up is to use high-precision timing information that can supplement the tracker and mitigate the impact of a high vertex density.

The High Granularity Timing Detector (HGTD) is proposed by the ATLAS experiment as part of the High Luminosity upgrade [1]. The recent development of Low Gain Avalanche Diodes (LGADs) and AC coupled LGADs (AC-LGADs) promises to significantly enhance the capability to measure track arrival times. These new detectors have have been chosen as the base detection technology of the HGTD because of their excellent timing performance, providing a < 30 ps time resolution.

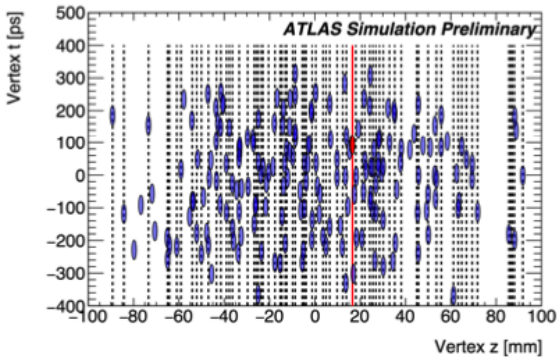

Figure 1.1: Simulation of primary vertices in an ATLAS event in the zt plane, showing the hard scatter (red ellipse) superimposed with about 200 pile-up interactions (blue ellipses). The dashed vertical lines represent the positions of reconstructed vertices.

At same time, the development of AC coupled Low Gain Avalanche Diodes (AC-LGADs) provides the necessary pixelation to improve the tracking performance with a pixel dimension of $\sim$ 200 μm x 200 μm. In this report we will focus on recent prototypes of AC coupled Low Gain Avalanche Diodes (AC-LGADs) built at Brookhaven National Laboratory.

The report is organized as follow: in the second chapter we will discuss the structure and the idea of LGADs and AC-LGADs; in the third chapter we will present the experimental set-up used to characterize the sensors; in the fourth we will focus on the results of the measure done in this internship and finally in the fifth chapter we'll wrap up some conclusions.

2. LGADs and AC-LGADs, a theoretical introduction

In this chapter we will focus our attention on the structure of the LGADs and the AC-LGADs. The studying of fast-timing detectors have attracted widespread interest in the scientific community around the world in relation to the development of the next generation of collider experiments and imaging techniques for a variety of applications.

2.1 LGAD

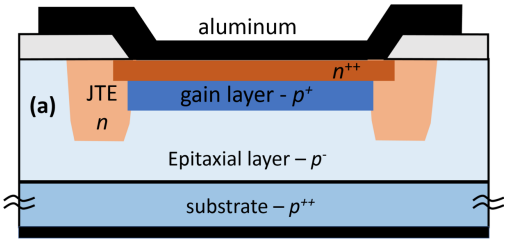

Figure 2.1: Sketch of the structure of an LGAD (not to scale). The GR termination is not shown.

The structure of a LGAD is shown in figure 2.1 [2]. The active volume of the device is an epitaxial layer or a thin silicon wafer-bonded to a thick substrate that acts as a mechanical support. The thickness of the epitaxial layer can be a few tens of m in order to have a short drift of the carriers.An n^{+}-layer creates the junction with the p-type substrate, as in a regular diode. In addiction, a p-layer is implanted just below the n^{+} implant (gain layer). Application of a bias to the junction leads to depletion of this layer which results in a high electric field in a superficial region that extends in depth for about a micron. Electron impact ionization is generated by this high field when the drifting electrons enter the gain layer volume, while the ionization rate of the holes is at a negligible level (thus excluding the onset of a breakdown). The result is an amplified current pulse which is dominated by the motion of the holes through the whole thickness of the substrate. These current pulses, amplified by a factor typically in the range 10- 20, are inherently fast and can offset the limited amount of charge released by a minimum ionizing particle (MIP) in the thin substrate (as compared to a standard 300 m thick silicon).

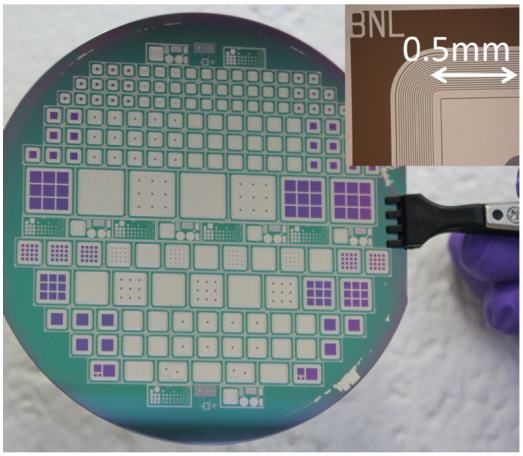

Figure 2.2: Photograph of a 4" wafer populated with single LGAD pads and arrays of LGAD pads. The inset on the top-right corner shows a close-up of an LGAD structure.

2.2 AC-LGAD

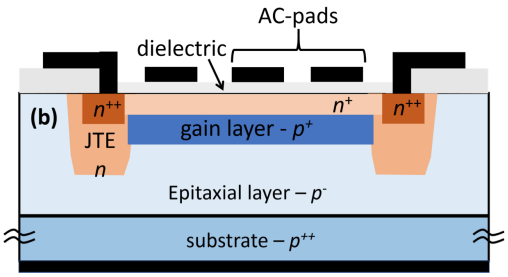

Figure 2.3: sketch of a section of a segmented AC-LGAD (not to scale).

The AC-LGAD is developed as a new paradigm in 4D tracking with fast-timing silicon detectors. In the actual fast-timing detectors design the isolation structures between readout pads represent a **no-gain** area. The physical limit to this "dead area" is about 30 μm.

A sketch of an AC-LGAD structure is shown in figure 2.3. In this type of device, metal electrodes are placed over an insulator at a fine pitch, and signals are capacitively induced on these electrodes[3].

In order to exhibit similar gains and in turn similar fast timing performance as the LGADs, AC-LGADs are fabricated on p-type substrates of the same thickness. Upon application of a bias voltage, uniformly implanted n++ and

gain layers assure parallel electric field lines extending into the bulk, and in turn spatial uniformity of the gain. One of the main differences between AC-LGADs and standard LGADs is the replacement in AC-LGADs of the n++ layer by a much less doped n+ layer. Moreover, the electrodes, which the read-out electronics is connected to, are metal pads separated from the n+ layer by a thin insulator.

In this design a highly-doping n++ implant is still present at the edge of the device and DC-connected to a voltage source for electron current draining. Electrons are first collected by the n+ layer and from it by an electrode contacting the n++ implant at the periphery of the device. The back of the device is uniform, and acts as an ohmic contact. Externally to the active area, a series of floating Guard Rings (GR) are included in the design.

Since AC-coupled electrodes do not collect charge, the current induced on the AC-LGAD pads is bipolar with zero net integral, with a first peak accounting for the drift of the multiplication holes into the substrate and a second peak, of opposite polarity, to account for diffusion of the electrons within the n+ toward the n++ contact at the edge of the device. Electrons collected at the n+ layer will then discharge slowly to the n++ contact, with a time constant given approximately by $R_{GND} \times C_{n+}$, where C_{n+} is the capacitance of the n+ layer towards the rest of the world. This time constant is much larger than the read-out time, so that the opposite polarity pulse amplitude is negligible.

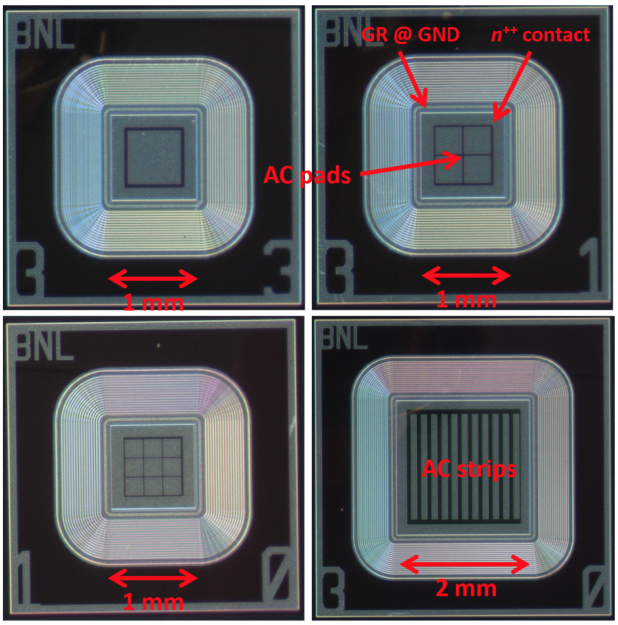

Figure 2.4: Photographs of different AC-LGAD structures: (top-left) single AC-pad 600 m 600 m active area, (top-right) 2 2 array with 300 m 300 m pads at 330 m pitch, (bottom-left) 3 3 array with 200 m 200 m pads at 220 m pitch, and (bottom-right) array of strips of 80 m width 1.5 mm length at 150 m pitch. The sizes of the active areas, the positions of the AC-coupled pads, the GR and n++ contacts are indicated with arrows.

3. Experimental set-up

In this chapter we will talk about the experimental set-up used to characterize the LGADs and the AC-LGADs. Within the RD50 collaboration at CERN, a characterization technique for testing the parameters of silicon detectors has been developed. This procedure is called Transient Current Technique (TCT) (Fig. 3.1, 3.2). It consists in a deployment of a fast pulsed laser to hit the Device Under Test (DUT) and is based on the analysis of the current induced by the movement of charge carriers inside a sensor. The current induced is amplified and time resolved using a wide band oscilloscope. Just by studying the shape of the induced current we can infer information of the doping, electric field and charge collection efficiency of the detector.

3.1 Transient Current Technique equipment

The equipment for TCT comprises different pieces: a laser for illuminating the DUTs, a system for monitoring the laser intensity, an IR camera to help positioning the direction of the laser, power supplies for providing the bias voltage to the DUT and remote controlled stages for moving the laser position respect to the DUT. Signal amplifiers, filters, a 5 GHz oscilloscope and a cooling system are also included in the setup.

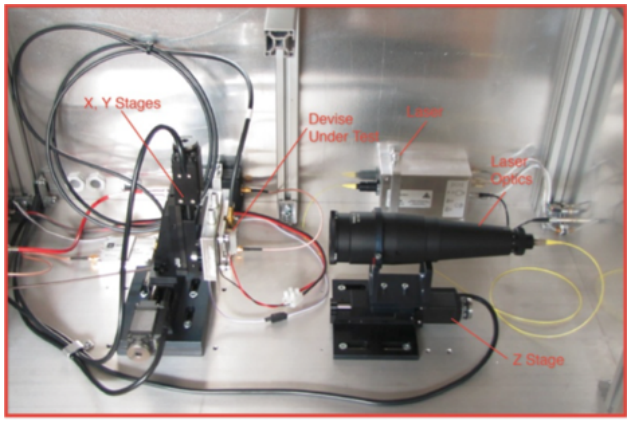

Figure 3.1: Physical setup of the TCT equipment.

Laser

Transient Current Technique deploys a pulsed laser to hit the silicon detector, depositing energy and triggering the detectors response similarly to what a

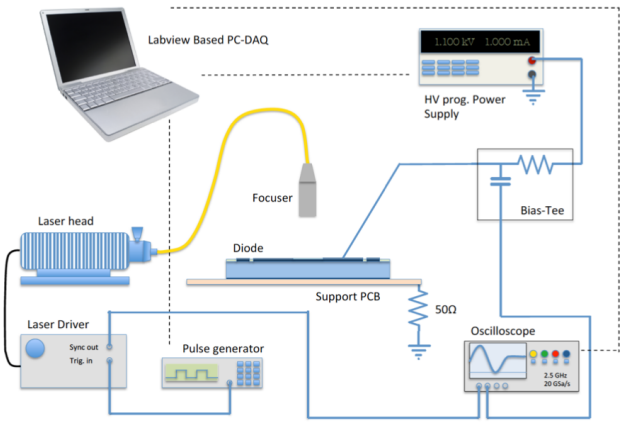

Figure 3.2: Schematics of a typical setup of the Transient Current Technique.

MIP would do. Two lasers with different wavelengths had been used: red and infrared. The specifics are shown in table 3.1.

Type	Diode Laser LA-01
Wavelength	1064 nm (IR) or 660 nm (RED)
Pulse power	few to 100s MIPs
Penetration depth on Si	1 mm (IR) or 10 μm (RED)
Running mode	50 Hz - 500 kHz

Table 3.1: Laser specifics

The infrared laser penetrates 1mm of silicon, therefore passes through the DUTs and generates a signal similar to several MIPs while the red laser has a low penetration depth into silicon, around 10μm (Fig. 3.3).

This means that the output signal from some devices is significantly different if the red laser hits the front of the detector rather than from the back. LGADs, for example, have the highly doped gain layer in the front side which would not be hit by a laser injected from the backside.

The laser at full power saturates the detector readout (500 mV), thus it has to be attenuated. This was done in two ways: by adding a neutral density filter in front of the laser optical lens and/or by regulating a current threshold through a Digital to Analog Controller (DAC) via software. Only the current that breaches the defined threshold is fed into the laser and

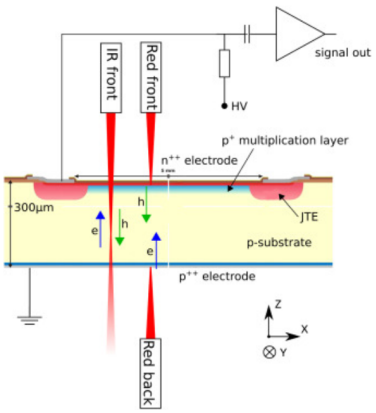

Figure 3.3: Schematics of a TCT example on an LGAD, showing the different penetration depths of the lasers deployed.

therefore the duration of the pulse is regulated (Fig. 3.4). To synchronize the data taking with the laser pulses, the signal from the laser pulse generator is also used for triggering. The trigger signal is negative and its amplitude is 500 mV after amplification (Fig. 3.5).

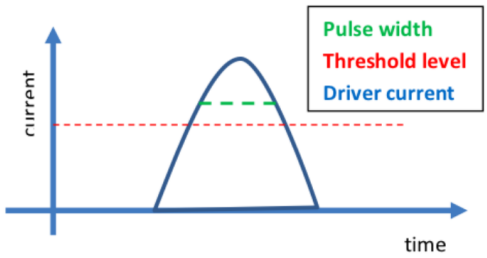

Figure 3.4: Laser current threshold. It is to be noted that the laser pulse duration does not scale linearly with the raise of the threshold due to the shape of the current pulse.

Beam monitoring

The beam monitoring apparatus BM-01 is used to monitor the beam intensity of the laser illuminating the DUT. In such a way it is possible to correct for variations of beam intensity (due, for example, to temperature changes) over long scans. The beam monitor consists in three parts: a beam splitter, a reverse biased diode with large area (few mm2) and circuitry for shaping and amplifying the signal from the diode (Fig. 3.6). The beam splitter is

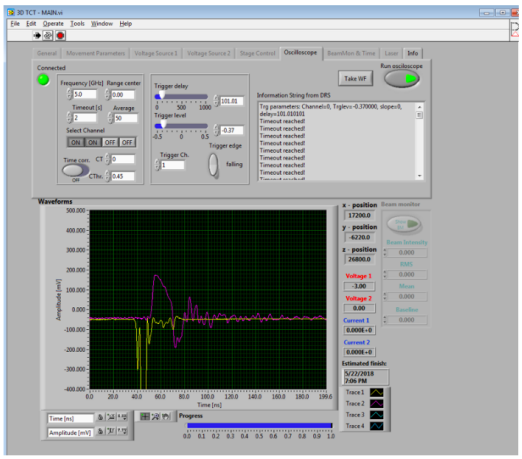

Figure 3.5: Screenshot of the graphical user interface for the TCT system. The output of the broadband oscilloscope is shown on a black background. Laser trigger (yellow) and waveform (purple).

mounted in front of the beam tilted by 45 and splits the beam in different ratios (70:30 or 50:50). The reflected beam hits a large area photodiode mounted on top of the beam splitter. The signal generated by the photodiode is readout by a channel of the oscilloscope. Since lasers of different wavelengths have different focal lengths (red, infrared), adjustment screws could be used to precisely set the position of the photodiode to ensure that the beam is illuminating the sensitive surface (Fig. 3.6).

Servo motor stages

The position of the laser relative to the detector is controlled by three servo stepper motor stages Standa 8MT30 (nominal resolution 0.156 m corresponding to 1/8 step). Two stages are attached to the sensors support allowing the movement of the detector along x and y axes. The third stage moves the laser optical support along z axis, thus regulating the distance of the source from the detector to adjust according to the focus of the laser (Fig. 3.7). All three stages are controlled by a dedicated LabVIEW program.

Oscilloscope

To record the signal waveforms a board called "DRS4" (fig. 3.8) designed by the Paul Scherrer Institut in Switzerland, was used. This board works

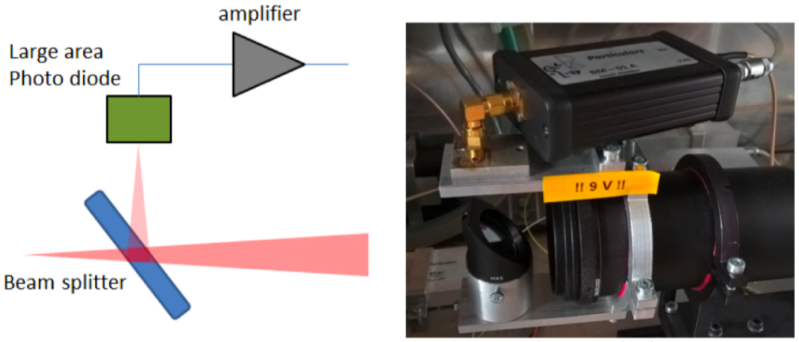

(a) TCT Beam monitoring schematics (b) TCT BM-01 mount

Figure 3.6: (a) Schematics of the beam monitoring BM-01: a splitter deflects a fixed fraction of the beam to a large area diode. Laser intensity can be inferred from the measurement of the charge collection of the diode. (b) Mount of the BM-01 apparatus with dedicated screws to allow fine adjustment of the position of the diode relative to the splitter.

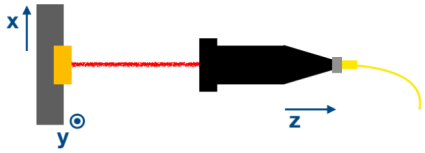

Figure 3.7: Sketch of stage positions. The X and Y axes stages move the device tested, Z stage moves the laser.

similarly to an oscilloscope connected with the computer and can be controlled and readout by a custom LabVIEW software. Three to four channels were used during the measurements: one for the signal coming from the laser trigger, one or two for the DUT output, and the third channel for the beam monitoring output. All the signals were amplified before being readout by the oscilloscope as stated previously.

Figure 3.8: The DRS4 board used as 1 GHz 4-channel oscilloscope.

3.2 FermiLab board

The sensors under test were wired bonded (see fig. 3.9) to a 16 channel Transimpedance Amplifier (TA) developed by the Fermilab National Laboratory. The board is characterized by a gain of ~ 140 and a bandwidth of $\sim$1 GHz. The board is shown in fig. 3.10.

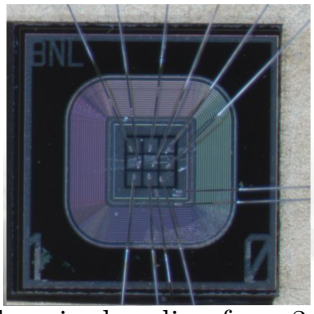

Figure 3.9: Example of the wire bonding for a 3x3 pixel matrix AC-LGAD.

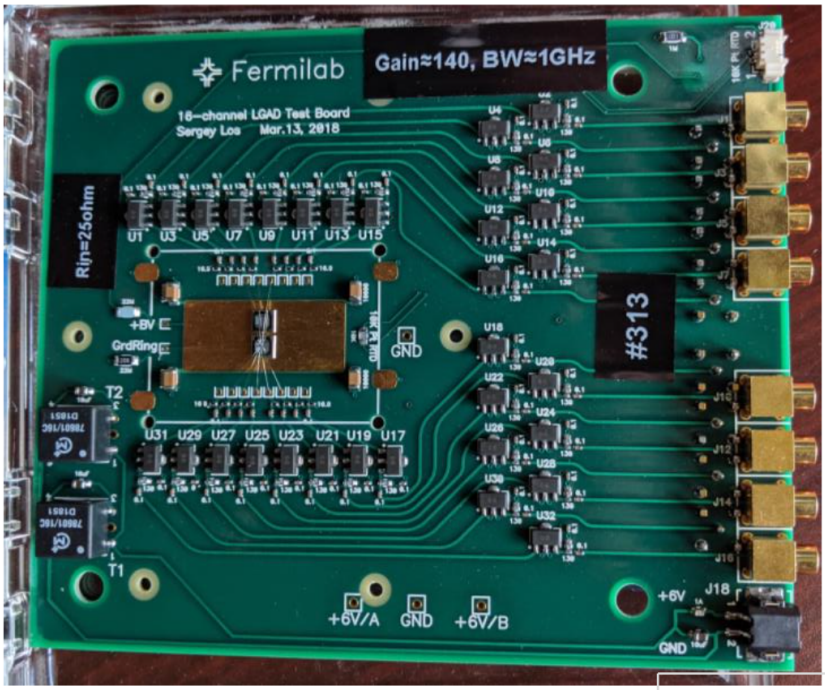

Figure 3.10: 16 channel TA board developed by Fermilab. In this picture there are two sensors glued to the board.

4. Measures, results and discussion

In this chapter we will present the measures and the results obtained in the training. In particular we will discuss about the tests on a single pad LGAD, on two different 3x3 pixel matrix AC-LGAD and on a 8 Strip AC-LGAD produced at BNL.

4.1 Calibration of the experimental set-up

The first challenge of this training was the calibration of the TCT setup. All the optics were aligned, in particular the beam monitoring system. The best alignment was obtained maximizing the readout signal of the beam monitoring diode.

After that, another important step was the characterization of the gain of the Amplifier used for the LGADs and for the diodes. The were two different amplifiers, the AM-01A and the AM-02A (fig. 4.1)from Particulars, they nominally differ only for the bandwidth, but we discover two different gain for the two amplifiers. In particular the AM-01A shows a gain of 52 dB @ 12 V, while the AM-01A shows a gain of 46 @ 15 V. In addiction the AM-01A shows more noise for high frequency signal so we choose to use only the AM-02A.

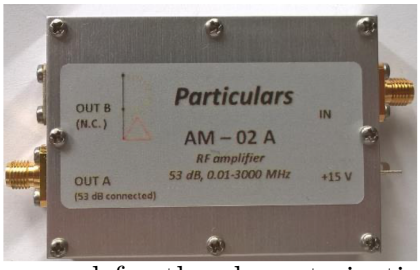

Figure 4.1: Amplifiers used for the characterization of diodes and single pad LGADs

4.2 Focus Scan

After the calibration we needed to verify the system so we started testing an already characterized LGAD.

Every time a new sensor is mounted on the TCT the first step pf the characterization is the focus scan. It consists in the focusing procedure of the laser, performed by moving the source at the optimal distance from the DUT. The procedure makes use of the area between the metallized and the non-metallized part on the detector surface while the silicon sensor is depleted.

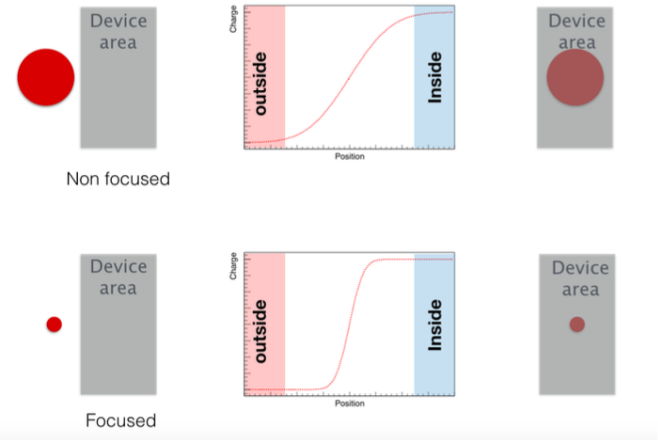

Figure 4.2: The FWHM of the error function of charge is smaller the more the laser is focused. It depends on the distance of the laser source from the device (z coordinate, optical distance). In order to focus the laser the minimum FWHM has to be found, varying the z coordinate.

The focus scan requires three main steps:

- **Sweep along optical axis (z) and along one between x and y**. In order to choose the optimum range of the scan we firstly do a visual focusing minimizing the dimension of the laser spot on the sensor using an IR camera. After that we do the sweep, in this particular cases we did a sweep along y (scan axis) and z at every 50 μm. For each point of the scan we can plot the waveform, as shown in figure 4.3;

- **Fit an error function on each waveform.** The plotted waveform are integrated and the results of this integration are plotted against the scan axis for every optical distances and this plots are fitted with an error function due to the gaussian shape of the laser spot profile (fig. 4.4);

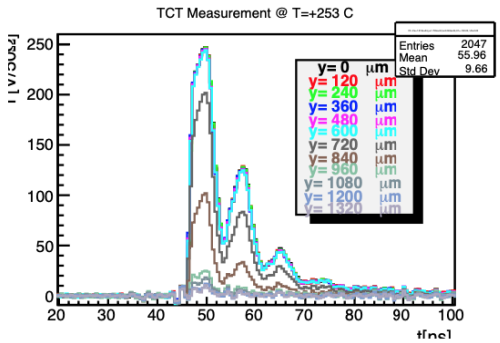

Figure 4.3: Waveforms acquired during a LGAD focus scan sweep at different y coordinates: the amplitude is proportional to the fraction of the laser spot hitting the sensor. When the laser is completely off the sensitive area of the sensor, the waveform is flat, i.e. no signal is observed above the instrumental noise.

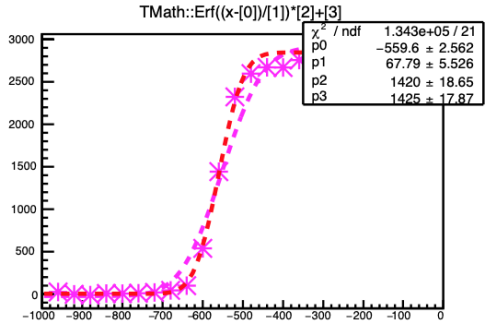

Figure 4.4: The collected charge for each sweep is fitted with an error function due to the gaussian beam of the laser.

- **Find the minimum of the Full Width at Half Maximum.** The sigma of the error function for every points along z is our FWHM, which is plotted against the optical distance. The plot shows a parabolic dependence (fig. 4.5), so its possible to minimize and find the optimum optical distance which corresponds the minimum dimension of the beam spot;

The last analysis that we can do with a focus scan is the test of the alignment of the laser on the optical axis. Plotted the position of the edge against the optical distance, the slope of the plot gives us the angle between the optical axis and the beam of the laser (fig. 4.6).

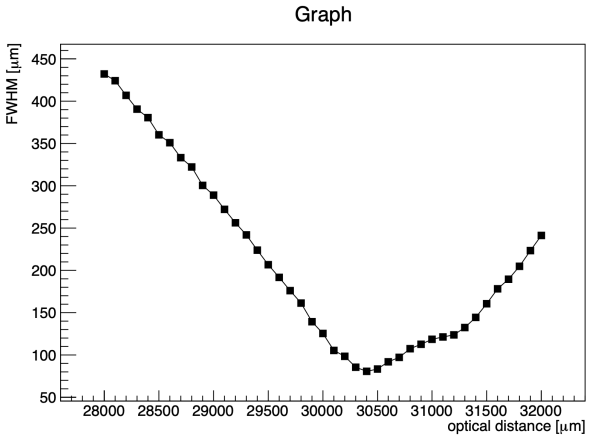

Figure 4.5: Focus scan result, with focus at a FWHM slightly above 50 μm at a relative coordinate z=30500 m.

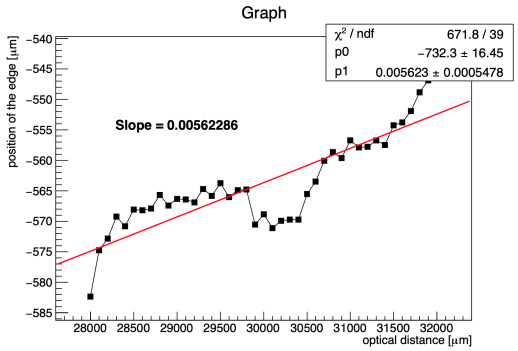

Figure 4.6: The slope of the plot gives as the angle between the optical axis and the beam of the laser, in this case the sensor is good aligned.

4.3 Pixel Map

Once the laser is focused, the z position of the stage is kept constant, and a series of waveforms are acquired varying the x and y coordinates following a rectangular grid. The charge collected, computed from the waveforms is plotted in a 2D-map which throughout this report is called pixel map.

The LGAD that we tested is an already full characterized LGAD, so we can validate the calibration of the TCT setup. In the picture you can see a scratch on the sensor already seen in the previous characterization of the sensor. At that moment we validated the operation of the TCT, so we could start the tests of the AC-LGADs.

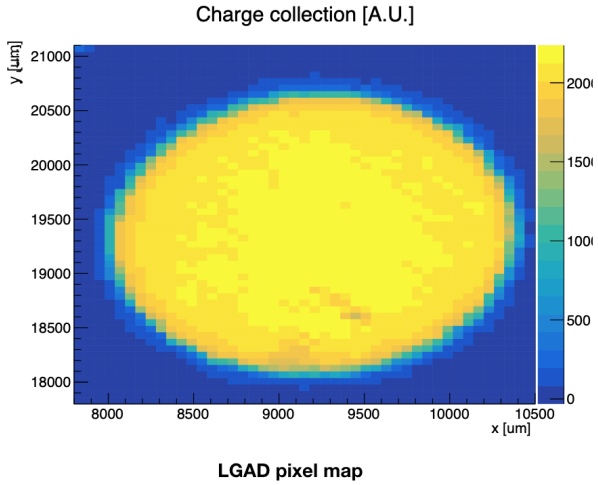

Figure 4.7: Pixel map from LGAD. Note the scratch on the sensor.

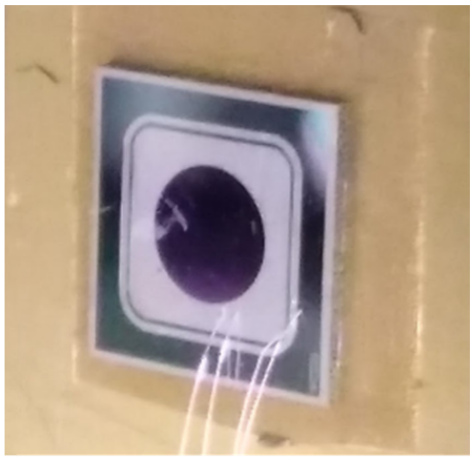

Figure 4.8: Photo of the LGAD under testing. You can note the scratch in the same position of the one visible in the pixel map.

4.4 AC-LGADs pixel matrix tests

In this report we will present the first characterization of an AC-LGAD with the TCT equipment. The first sensor that we tested is a 3 * 3 pixel matrix AC-LGAD, every pixel is 200 μm * 200 μm and the distance between two pixel is 20 μm (fig. 4.9).

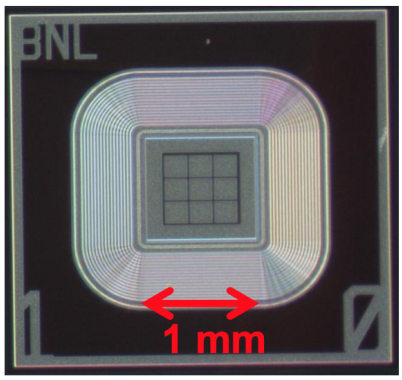

Figure 4.9: Photo of the first AC-LGAD we tested.

4.4.1 Focus Scan and Pixel Map

We followed the same test procedure used for the LGAD, so the first measure was the Focus Scan. We performed various scans changing the step along

the optical axis and finally we obtained a spot diameter of less than 20 μm at $z = 37400$ (fig. 4.10). We did the pixel map both with red and IR laser and we obtained the similar results as you can see in the picture 4.11.

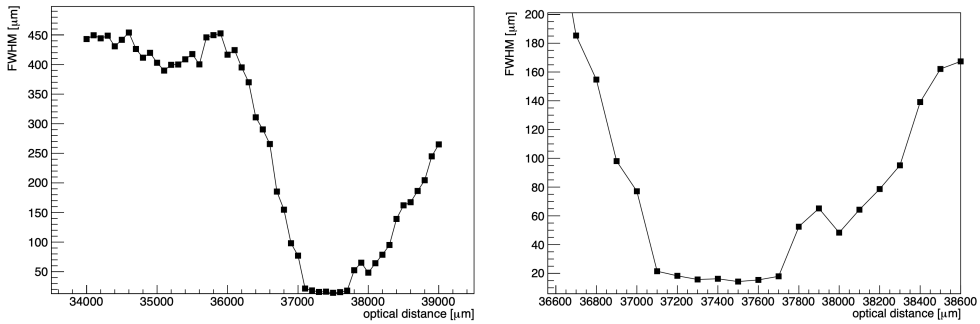

Figure 4.10: On the left the FWHM against the optical distance, it's possible to see the minimum of the distribution. On the right a zoom of the minimum region, showing a FWHM of less than 20 μm at z=37400.

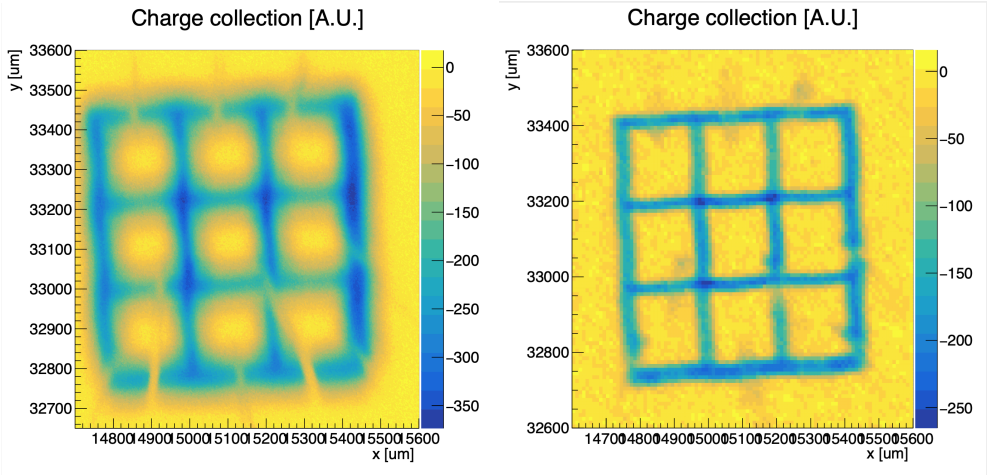

Figure 4.11: On the left the pixel map of the AC-LGAD with the IR laser and a pixel of 2 μm, it's possible to see the wire bondings of the single pixels. On the right the pixel map with the Red laser and a pixel of 10 μm.

4.4.2 Cross-talk

In [3] the group presented the first measure of the Cross-talk for an AC-LGAD. That measure was obtained with a Strontium 90 beta source, so we

tried to do the repeat the test for validation and we tried to do the same test with the TCT equipment.

With the ^{90}Sr source we record the signal of a triggering pixel, a near and a far pixel (fig. 4.12) and we obtained the results shown in figure 4.13 and in table 4.1.

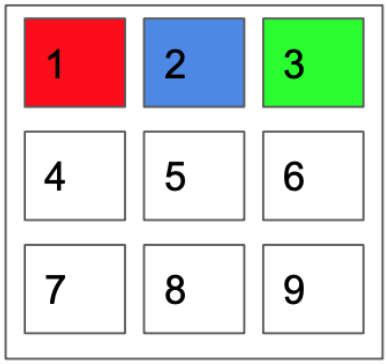

Figure 4.12: The red pixel is the triggering pixel (we set a trigger of -100 mV), the blue one is the near and the green is the far pixel.

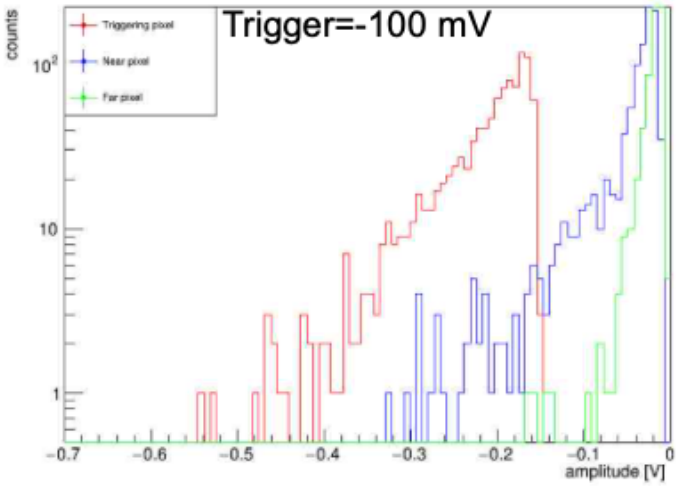

Figure 4.13: Spectra of the amplitude of signals produced by beta radiation from a 90Sr source for three channels in the 3 3 array of AC-LGAD pixels in figure 4.9. On the sensor a bias voltage of 80 V was applied and a trigger threshold of 100 mV was set on the scope on the triggering channel.

$V_{min}^{Near}/V_{min}^{Trigg}$	0.22
$V_{min}^{Far}/V_{min}^{Trigg}$	0.08

Table 4.1: Mean value of the distribution of the ratios between near (far) and triggering pixel. The uncertainty is on the last digit.

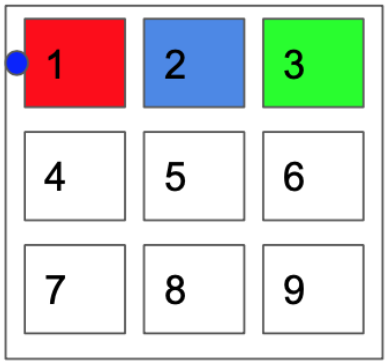

Figure 4.14: Example of laser placement for cross-talk measurement with laser.

To perform the laser tests (firstly with the IR laser) we positioned the laser as shown in figure 4.14, in the center of the side of the triggering pixel and we read the output signal triggering, near and far pixel.

The first measures showed an unexpected result, indeed the far pixel showed an output signal bigger than the one read on the near pixel.

To explain this phenomena we need to analyze again the pixel map. If we integrate the waveform only in the time interval where there is the electron signal we obtain a new pixel map (fig. 4.16) that really shows the signal read by the test pixel. As you can see, the signal is maximized around the pixel and all around the sensor, showing an edge effect that cause the abnormal results shown in the cross-talk.

This edge effect is completely unexpected so we tried to understand the origin of this effect. If we schematize the AC-LGAD with a circuital model (fig. 4.17), we can see that the pixels along the edge are all at the same potential so the signal flow from one pixel to the others. To minimize this edge effect we need to increase the resistivity of the n+ layer along the edge.

After that we tried to understand better the cross-talk of this sensor so we

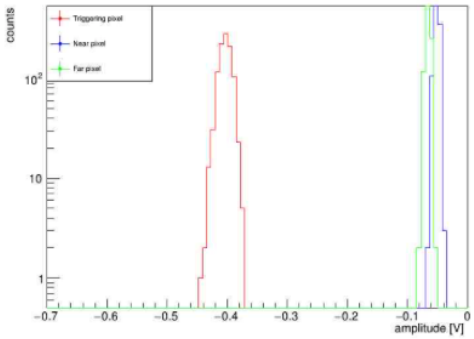

Figure 4.15: Spectra of the signal amplitude produced by the IR laser on the AC-LGAD. The signal produced on the far pixel was greater that the one produced on the near pixel. In particular $V_{min}^{Near}/V_{min}^{Trigg} = 12,6\%$ and $V_{min}^{Far}/V_{min}^{Trigg} = 16,2\%$.

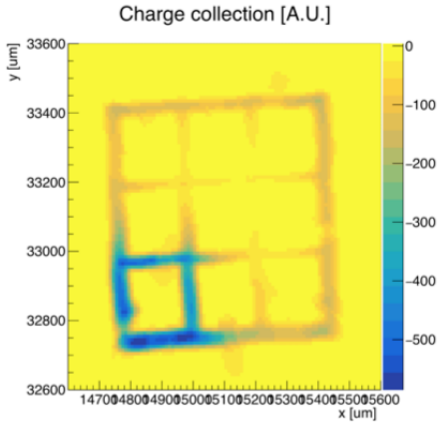

Figure 4.16: Pixel map of the AC-LGAD with a correct integration of the waveform.

did multiple tests changing the combination of triggering, near and far pixel and we obtained the results showed in the graph (fig.4.18).

To prove that the cross-talk depends on the resistivity of the n+ layer we did the same measures with a new AC-LGAD with a different implantation dose for the n+ layer.

The results in table 4.2 shows an evident difference between the two sensors, indeed in the region where the resistivity is lower the cross-talk decreases

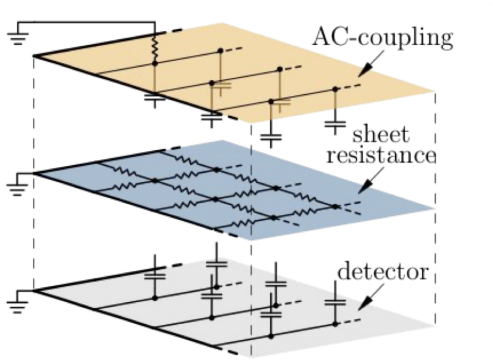

Figure 4.17: Circuital model of the AC-LGAD.

	Dose n+ 1/10	Dose n+ 1/100
$V_{min}^{Near}/V_{min}^{Trigg}$	9%	7%
$V_{min}^{Far}/V_{min}^{Trigg}$	16%	11%

Table 4.2: Ratios for two different AC-LGADs with different implantation dose along the edge of the n+ layer.

while where the resistivity is the same the cross-talk doesn't change so much. These results suggest the possibility to tune the dose in order to obtained the desired cross-talk.

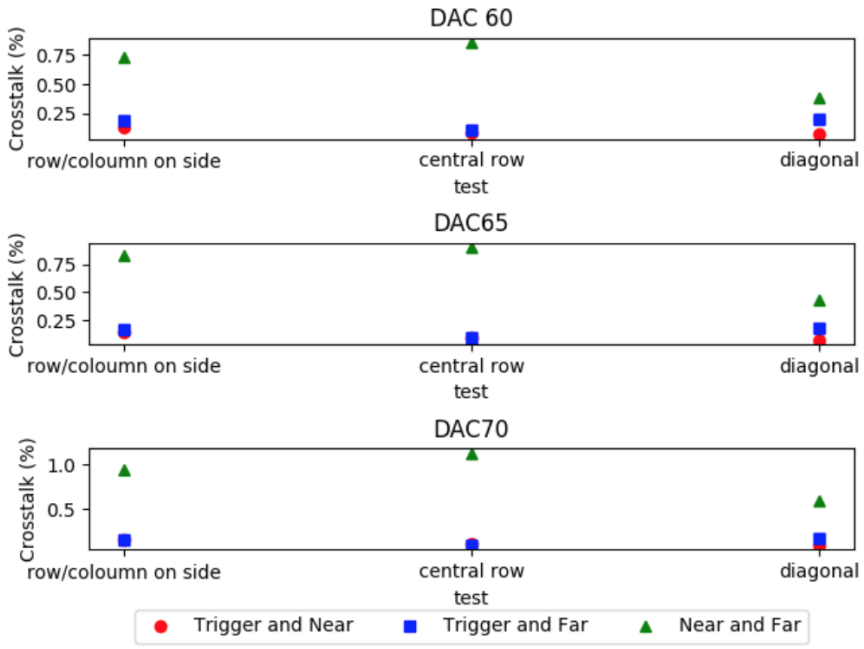

Figure 4.18: Graph of the cross-talk for different pixels combinations. There is a big difference in the cross-talk ratios for the rows on the edge and for the central row due to the edge effect. In addiction there is a big difference with a diagonal combination due to the greater distance between the pixels.

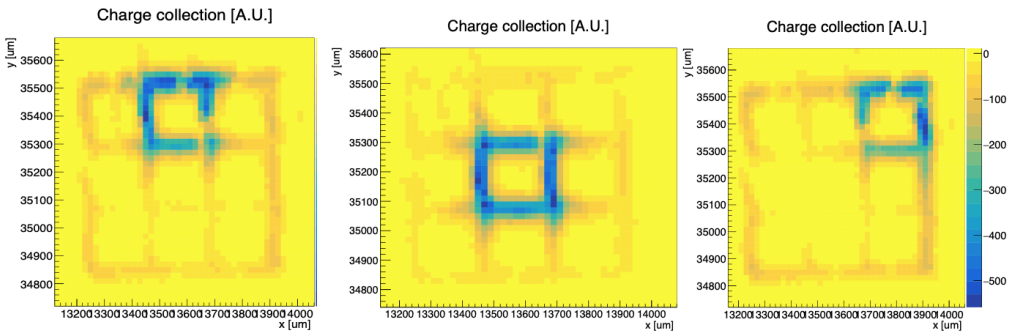

Figure 4.19: Pixel map of the AC-LGAD with a different implantation dose for the n+ layer.

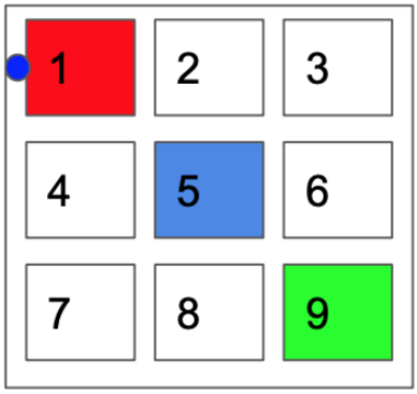

Figure 4.20: Pixels under test to understand the cross-talk dependence on the resistivity of the n+ layer.

4.5 AC-LGADs strip tests

The last sensor that we tested was a 8 strip AC-LGAD, shown in figure 4.21, every strip is 80 μm width and 1400 μm long; the distance between the strip is 120 μm. This strip sensor is from the same silicon wafer of the second AC-LGAD that we tested so we expected similar results.

4.5.1 Focus Scan and Pixel Map

As done for the other sensor, firstly we did a Focus Scan and a Pixel Map of the sensor. In the figure 4.22 you can see the results of the pixel maps; as you can see we integrate the waveforms for the pixel maps in the right time interval and we obtain the same edge effect seen in the other devices.

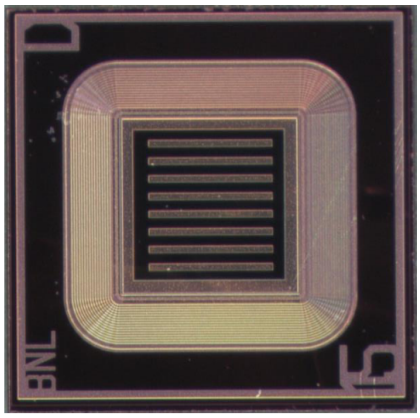

Figure 4.21: Photo of the strip sensor under test.

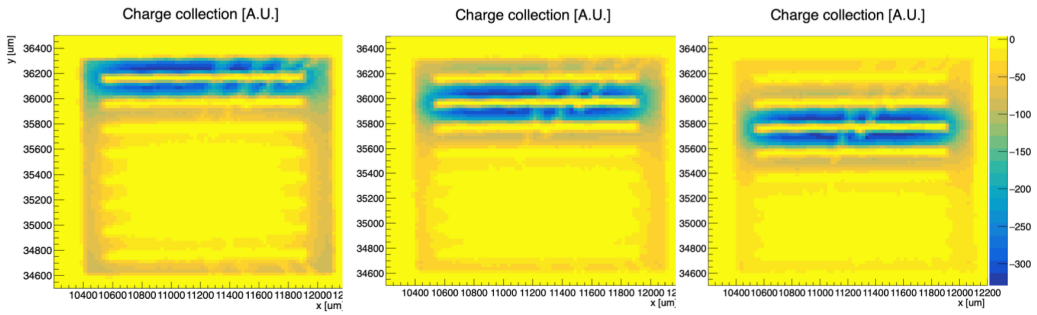

Figure 4.22: Pixel map of the strip sensor under test. We can see a clear edge effect on the sensor. The resistivity of the n^+ layer is lower so we don't have the same effect in the center of the sensor, but only along the edges.

4.5.2 Cross-talk

Finally, we did the measure of the cross-talk of the strip sensor.

We set the position of the laser between the first two strips in order to reduce the edge effect and we measure the signal read by 4 strips (fig. 4.23) because we were limited by the available number of DAQ channel. By varying the readout strips we measured the trend of the cross-talk. You can see the results in the plot. The cross-talk decrease quickly to ~ 0, indeed the signal on the last strips is just ~ 5 mV, which is the level of the noise for our system.

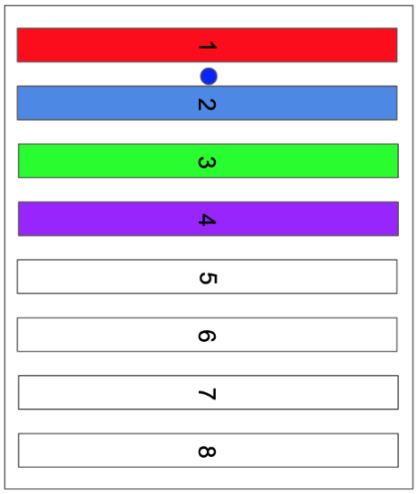

Figure 4.23: Example of scheme of the cross-talk measurement for strip sensor. The red strip is the triggering one. We were limited by the DAQ system to 4 strips at a time, so we repeated the measurement with different strips in order to scan all the trend.

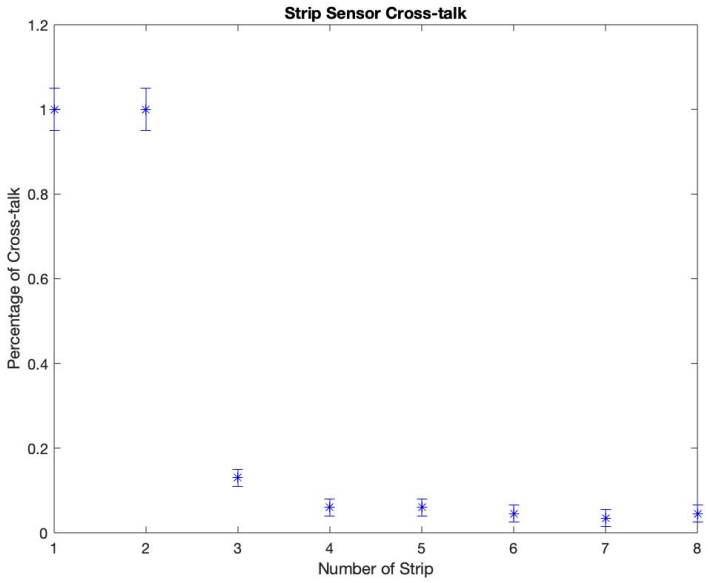

Figure 4.24: Trend of the Cross-talk for the strip sensor. The cross-talk on the last strips is practically zero because the signal is approximately equal to the noise of the system.

5. Conclusion

In this report we presented the results of the first full characterization of the BNL made AC-LGAD.

The AC-LGAD is a new type of detector developed to overcome the limitation of the LGADs, indeed in the AC-LGAD the active area of the sensor is 100% and the fine pixelation improve the spatial resolution whereas the time resolution is comparable with the LGAD one.

In particular in this training we obtained the first measure of an AC-LGAD with the TCT equipment, this setup let us to discover an edge effect in the AC-LGAD that will be corrected in the next generation of devices.

In conclusion we can say that:

- The TCT is a good probe station for the LGADs and the AC-LGADs;
- The AC-LGADs produced at BNL are good sensors that need only a tuning of the implantation dose for the gain layer in order to improve the cross-talk performance.

In the next future the timing resolution of the AC-LGADs will be tested with a setup developed at BNL that let us to measure the different time arrival of a coincidence signal produced by a Strontium 90 beta source on two sensors, one used as trigger and the other one used as device under test.

Bibliography

[1] Atlas Collaboration. Technical Proposal: A High-Granularity Timing Detector for the ATLAS Phase-II Upgrade. *CERN-LHCC- 2018-023 LHCC-P-012*, 2018. 1

[2] Francesco Lanni Alessandro Tricoli Gabriele Giacomini, Wei Chen. Development of a technology for the fabrication of Low-Gain Avalanche Detectors at BNL. *NIMA 62119*, 2019. 3

[3] Gabriele D'Amen Alessandro Tricoli Gabriele Giacomini, Wei Chen. Fabrication and performance of AC-coupled LGADs. *JINST*, 2019. 4, 20